AUTOMATED PIPELINE EXTRACTION FROM INTERFEROMETRIC SAR DATA OF THE ERS TANDEM MISSION*

Olaf Hellwich[1], Ivan Laptev[2] and Helmut Mayer[1]

[1]Chair for Photogrammetry and Remote Sensing
[2]Forschungsgruppe Bildverstehen, Informatik IX

Technische Universität München, D-80290 Munich, Germany

E-mail: {olaf|helmut}@photo.verm.tu-muenchen.de; laptev@informatik.tu-muenchen.de
URL: http://www.photo.verm.tu-muenchen.de

Commission VII, Working Group VII/6

KEY WORDS: SAR Interferometry, Data Fusion, Line Extraction, Markov Random Field, Snakes

ABSTRACT

A new method for the automated extraction of pipelines and roads from Synthetic Aperture Radar (SAR) scenes is presented. It combines intensity data with coherence data from an interferometric evaluation of a SAR scene pair. The fusion is based on Bayesian statistics and part of a Markov random field (MRF) model for line extraction. Both, intensity and coherence data are evaluated using rotating templates. The different statistical properties of intensity and coherence are taken into account by a multiplicative noise model and an additive noise model, respectively. The MRF model introduces prior knowledge about the continuity and the narrowness of lines. Posterior odds resulting from the MRF method are input to a ziplock snake-based method for linear object extraction. This processing step is controlled interactively which seems to be necessary as long as fully automatic processing of noisy data does not provide sufficiently predictable results. The method is applied to data of the ERS tandem mission.

1 INTRODUCTION

The extraction of linear objects like roads, rivers and pipelines from SAR data is of great practical interest, because of the all-weather availability of SAR data. Its automation is not easy owing to the general speckle effect and "no-show" effects special to linear features (Leberl, 1990). The newly developed method for linear object extraction tries to compensate for these defects as follows: SAR intensity and interferometric coherence data are combined in a Bayesian data fusion. An MRF model is used to bridge line gaps caused by speckle effects, thus considering the characteristics of SAR data. In the following processing, object extraction methods primarily developed for optical data are applied. Here, interactively initialized ziplock snakes are used for pipeline extraction.

In the following two sections the basics of MRF- and snake-based line extraction are explained. Then the method is applied to an ERS tandem data set from the Siberian lowlands for pipeline extraction.

2 MRF-BASED LINE EXTRACTION

Previous investigations have shown (Hendry et al., 1988, Hellwich and Streck, 1996) that SAR intensity and coherence contain complementary information about linear objects. Over the whole scene both data sources are only weakly correlated. Visual inspections reveal that linear objects are often only visible in either intensity or coherence. To fuse the information contained in both data sources an automatic method for data fusion was developed based on a Bayesian approach.

*This research was partially funded by Deutsches Zentrum für Luft- und Raumfahrt DLR e.V. under contract 50EE9423.

According to Bayes' theorem

$$p(\varepsilon|\boldsymbol{y}) \propto p(\boldsymbol{y}|\varepsilon)p(\varepsilon) \tag{1}$$

the *a posteriori* probability density $p(\varepsilon|\boldsymbol{y})$ of the object parameters ε given the observations $\boldsymbol{y}$ is proportional to the product of the probability density $p(\boldsymbol{y}|\varepsilon)$ of the observations given the object parameters and the *a priori* probability density $p(\varepsilon)$ of the object parameters. Considering that the observations are a constant in the estimation of object parameters, $p(\boldsymbol{y}|\varepsilon)$ is also called likelihood function (of the object parameters).

Bayes' theorem can also be applied recursively by using the *a posteriori* probability density $p(\varepsilon|\boldsymbol{y_1})$ belonging to the vector of observations $\boldsymbol{y_1}$ as *a priori* probability density for the evaluation of a second vector of observations $\boldsymbol{y_2}$ (Koch, 1990, p. 8). If $\boldsymbol{y_1}$ and $\boldsymbol{y_2}$ are conditionally independent, the *a posteriori* probability is given by

$$\begin{aligned} p(\varepsilon|\boldsymbol{y_1},\boldsymbol{y_2}) &\propto p(\boldsymbol{y_2}|\varepsilon)p(\varepsilon|\boldsymbol{y_1}) \\ &\propto p(\boldsymbol{y_2}|\varepsilon)p(\boldsymbol{y_1}|\varepsilon)p(\varepsilon). \end{aligned} \tag{2}$$

In the newly developed method for line extraction the observation vectors $\boldsymbol{y_1}$ and $\boldsymbol{y_2}$ contain values of the pixels of the SAR intensity and coherence images. The object parameters ε to be estimated for each pixel are the line or no-line state and - in case of the line state - the line direction. The *a priori* probability density $p(\varepsilon)$ of the object parameters is formulated as an MRF. In MRF the probability of a state in a pixel s does not depend on the states of all other pixels of the image, but only on the states of pixels belonging to a neighbourhood ∂s of s.

The goal of processing is the computation of a vector of object parameters, i.e. line states and directions as well as no-line states for the pixels of the image, for which $p(\varepsilon|\boldsymbol{y_1},\boldsymbol{y_2})$

is maximum or at least very high. In MRF this can be achieved with the help of various methods manipulating local probability densities. In this work, the local highest confidence first (LHCF) algorithm (Chou et al., 1993) has shown the best performance with respect to detection quality and computational speed.

Using the equivalence of MRF and neighbour Gibbs fields (Geman and Geman, 1984, Winkler, 1995), Bayes' theorem (1) can be formulated for the local probability density in a single pixel s:

$$p(\varepsilon_s|\partial\varepsilon_s, y_s) \propto p(y_s|\varepsilon_s) \cdot p(\varepsilon_s|\partial\varepsilon_s). \tag{3}$$

In neighbour Gibbs fields probabilities are expressed as a function of energies H:

$$p(x) = \frac{1}{Z} \exp\{-H(x)\} \tag{4}$$

where Z is a normalizing constant. With (4), instead of probabilities energies can be used:

$$H_s(\varepsilon_s|\partial\varepsilon_s, y_s) = H_s(y_s|\varepsilon_s) + H_s(\varepsilon_s|\partial\varepsilon_s). \tag{5}$$

In the following the computation of the different energy terms will be treated. A complete description of the method can be found in (Hellwich, 1997).

2.1 Data Evaluation

Line extraction is conducted using a template which consists of a line zone and two neighbouring side zones (Lopes et al., 1993). The simple line model assumes that the backscatter properties are homogenous in the line zone as well as in the side zones. To evaluate the image data the template is centered at each pixel. The likelihood that the center pixel of the template has the line state rises if the contrast between the line zone and both side zones increases. A contrast between the side zones is permitted. By rotating the line zone different line directions are treated. The data evaluation for each pixel results in the energy term $H_s(y_s|\varepsilon_s)$ where y_s is not a grey value of a pixel but a measure of the contrast between line and side zones, i.e. a derived observation. H_s is computed for both intensity and coherence.

2.1.1 Intensity SAR intensity has a multiplicative noise model (Goodman, 1975, Caves, 1993). Therefore, the normalized intensity ratio r as a measure of contrast between two homogeneous regions has a constant false alarm rate. It is given by

$$r = \min\left(\frac{\bar{I}_1}{\bar{I}_2}, \frac{\bar{I}_2}{\bar{I}_1}\right) \tag{6}$$

where $\bar{I}_1$ and $\bar{I}_2$ are the mean intensities of both regions.

The result of the evaluation of a template for a specific line direction is the maximum of the two normalized intensity ratios between the line zone and the side zones. This is a derived observation r_s in pixel s. Hence, the energy is given by

$$H_s(r_s|\varepsilon_s) = \begin{cases} \frac{r_s^2}{2\sigma_r^2} & \text{if } \varepsilon_s \in L \\ \frac{t_r^2}{2\sigma_r^2} & \text{if } \varepsilon_s = N \end{cases} \tag{7}$$

where σ_r is a constant, and t_r is a threshold balancing the no-line state versus the line states. L is the set of line states with different line directions, and N is the no-line state.

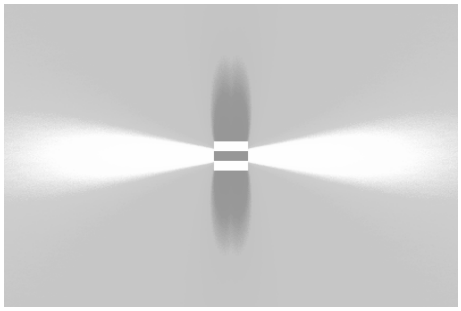

Figure 1: Model of the influence of a line pixel with horizontal direction. In the light irradiated field it supports, in the dark field it inhibits line pixels.

Eq. (7) was inspired by normally distributed observations. Empirical investigations (Hellwich, 1997) have shown that it sufficiently agrees with the theoretically derived probability density of the normalized intensity ratio between homogeneous regions with a known contrast (Lopes et al., 1993, Caves, 1993).

2.1.2 Coherence For coherence an additive noise model is considered appropriate (cf. (Tough et al., 1994)). Therefore, the difference d of the mean coherence values having a constant false alarm rate was used as a measure of contrast between the regions. The derived observation d_s for a pixel s is the minimum of the coherence differences between the line zone and both side zones. Corresponding with (7) the energy for differences d_s is computed from

$$H_s(d_s|\varepsilon_s) = \begin{cases} \frac{(d_s-\mu_d)^2}{2\sigma_d^2} & \text{if } \varepsilon_s \in L \\ \frac{(t_d-\mu_d)^2}{2\sigma_d^2} & \text{if } \varepsilon_s = N \end{cases} \tag{8}$$

where μ_d is a very large coherence difference occurring in the evaluated data. It can be set relatively arbitrarily. t_d is a threshold balancing the no-line state versus the line states. σ_d is used for weighting the coherence data with regard to the intensity data.

2.2 Markov Random Field Model

As the MRF model is not essential for the fusion of the two data sources, it is described very briefly only. The purpose of the model is the detection of continuous, thin lines. It is designed to bridge speckle-related (short) gaps interrupting the lines.

According to the model, each pixel with line state influences pixels in its neighbourhood. In a line pixel's direction it supports the presence of line pixels with a corresponding line direction. The effect of this influence is a stronger line continuity, i.e. a closing of gaps. Perpendicularly to its direction a line pixel inhibits the presence of line pixels with the same direction, thus preventing the occurance of thick lines. These two types of influences a line pixel puts on its neighbourhood are modelled with the help of completion fields (Williams and Jacobs, 1995) which the pixel "radiates" (cf. Fig. 1). The two parameters of the model control the strengths of the line supporting and the line inhibiting fields. They are also used to weight the influence of the MRF prior with respect to the data.

Summarizing, line extraction is controlled by the parameters t_r, t_d, and σ_d for data evaluation, and the line supporting and the line inhibiting parameter of the MRF model.

Using a training data set optimal parameters can be determined by simulated annealing (Hellwich, 1998).

Results are line pixels with line directions and no-line pixels, and posterior odds of the most probable line state versus the no-line state for each pixel. The latter are used for snake-based linear feature extraction explained in the next section.

3 SNAKES

This Section is based on (Laptev, 1997), where details of the approach can be found.

3.1 Basics of Snakes

The concept "snake", also called "active contour model", was originally introduced in (Kass et al., 1987). It combines internal smoothness constraints like bending of a curve with image forces like the gradient. This idea can be represented as a sum of its energies

$$E(\vec{v}) = E_{img}(\vec{v}) + E_{int}(\vec{v}) \tag{9}$$

where E_{int} represents the *internal energy* and E_{img} the *image energy*. The position of the snake where all these forces compensate each other corresponds to the local minimum of the snake's total energy E. Thus, the problem of the optimization of the snake's position is equivalent to the minimization of its energy.

The image energy of the snake can be defined as:

$$E_{img}(\vec{v}) = -\int_0^1 P(\vec{v}(s,t))ds, \tag{10}$$

where $P(\vec{v}(s,t))$ is a function with high values corresponding to the features of interest. When attracting the snake to edges in images, $P(\vec{v}(s,t))$ is usually taken equal to the magnitude of the image gradient, that is

$$P(\vec{v}(s,t)) = |\nabla I(\vec{v}(s,t))|, \tag{11}$$

where $I(\vec{v}(s,t))$ is the raw image or – more often – the image convolved with the Gaussian kernel. The convolution with a Gaussian kernel smoothes the image and removes disturbances which prevent the snake from moving toward the positions with lower image energy corresponding to the more salient image features.

The internal energy makes it possible to introduce geometric constraints on the shape of the snake. It can be defined as

$$E_{int}(\vec{v}) = \frac{1}{2}\int_0^1 \alpha(s)\left|\frac{\partial\vec{v}(s,t)}{\partial s}\right|^2 + \beta(s)\left|\frac{\partial^2\vec{v}(s,t)}{\partial s^2}\right|^2 ds, \tag{12}$$

where $\alpha(s)$ and $\beta(s)$ are arbitrary functions that control the snake's tension and rigidity. The constraint on tension is introduced by the first order term and makes the snake act like a membrane. The rigidity is constrained by the second order term and makes the snake act like a thin plate.

In order to find the optimal position for the snake, its energy has to be minimized. According to the variational calculus this must be a solution to the *Euler-Lagrange* differential equation of motion. When choosing a particular deformation energy the differential equation controling the motion of the snake becomes linear and can be separated. This has the advantage of solving one optimization step in linear time. For the actual implementation the equations have to be discretized. For details of this refer to (Laptev, 1997).

3.2 Ribbon Snakes

The goal of this paper is to extract linear features with significant width. They can be modeled by ribbons whose sides correspond to the features' boundaries. Using ribbon snakes, linear features can be extracted by optimizing the position and the width of the ribbon. In order to represent ribbon snakes, the parametric curve $\vec{v}(s,t)$ can be augmented by a third component $w(s,t)$ (Fua and Leclerc, 1990):

$$\vec{v}(s,t) = (x(s,t), y(s,t), w(s,t)), \qquad (0 \le s \le 1), \tag{13}$$

Such representation implies that each slice of the ribbon snake $\vec{v}(s_0,t_0)$ is characterized by its width $2w(s_0,t_0)$ and the location of its center $(x(s_0,t_0), y(s_0,t_0))$. All center points compose the centerline of the ribbon (cf. Figure 2 (a)).

In order to perform the optimization of the ribbon snake, the forces which act on it have to be defined. The advantage of the ribbon's representation in equation (13) is that the expression for the snake's internal energy E_{int} can be directly used for ribbon snakes. Doing so, the width of ribbons will be constrained by tension and rigidity in the same way as the two coordinate components. The internal forces which act on the ribbon snake will on the one hand constrain the ribbon's centerline to be a smooth curve. On the other hand, they will control the distance between the ribbon's sides, forcing the sides to be parallel.

In contrast to the original snakes, the image information for ribbon snakes has to be taken into account not at the center of the curve $(x(s,t), y(s,t))$, but at the ribbon's left and right sides. As shown in Figure 2 (a), for each slice of the ribbon $\vec{v}(s_0,t_0)$ there exist two points $\vec{v}_L(s_0,t_0)$ and $\vec{v}_R(s_0,t_0)$ corresponding to the ribbon's left and right sides. Adapting the expression for image energy E_{img} in equation (10) to ribbon snakes, the function $P(\vec{v}(s,t))$ in equation (11) has to be redefined. Requiring the image contrast to be large along the left and the right side of the ribbon, P can be defined as the sum of the image gradient magnitudes on the left and right ribbon sides:

$$P(\vec{v}(s,t)) = |\nabla I(\vec{v}_R(s,t))| + |\nabla I(\vec{v}_L(s,t))| \tag{14}$$

However, when searching for linear features which are known to be brighter or darker than their surroundings, the result of the extraction can be improved if the direction of image gradients at the left and right sides of the ribbon will be taken into consideration, too. For example, the extraction of bright linear features implies that the image intensity at the ribbon sides has to change from dark to bright at the left ribbon side and from bright to dark at its right side (cf. Figure 2 (b)). This is equivalent to demanding the projection of image gradient on the vector $\vec{n}(s,t)$ to be negative along the ribbon's left side $\vec{v}_L(s,t)$ and positive along its right side $\vec{v}_R(s,t)$. Taking this into account, the function $P(\vec{v}(s,t))$ can be redefined as

$$P(\vec{v}(s,t)) = (\nabla I(\vec{v}_L(s,t)) - \nabla I(\vec{v}_R(s,t))) \cdot \vec{n}(s,t). \tag{15}$$

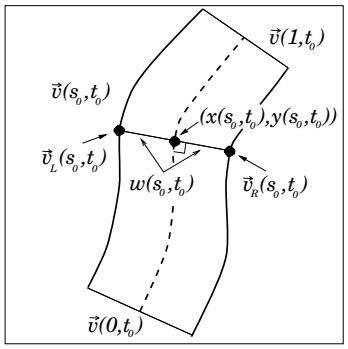

(a)

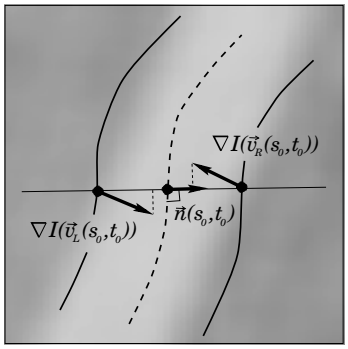

(b)

Figure 2: (a) Parametric representation of the ribbon snake. Each slice $\vec{v}(s_0, t_0)$ is identified by center $(x(s_0, t_0), y(s_0, t_0))$ and width $2w(s_0, t_0)$. (b) Image gradients for the two sides of the ribbon and their projection onto the ribbon's unit normal vector $\vec{n}(s_0, t_0)$.

3.3 Ziplock Principle

A problem often encountered is the following: to make interaction as efficient as possible only the end points of the snake are given manually. The direct straight connection of these end points can – especially close to the center – be far off from the linear object to be extracted by the snake. When optimizing the whole snake at a time this is not only ineffective, but the snake can also get stuck in local minima. To overcome this, the "ziplock" method was introduced in (Neuenschwander et al., 1995). There, the information is gradually propagated from the ribbon's ends towards its center by optimizing only parts of the snake at a time while approaching the center. The curvature of the snake is constrained to be low. By this means the "active" parts of the snake remain close to the linear feature during the whole optimization. The whole snake and the linear feature behave like a ziplock which is closed from both ends.

4 RESULTS

A part of an ERS tandem data set from the Siberian lowlands is used to demonstrate the new method. It contains straight pipelines and roads. Figure 3 shows the magnitude and Figure 4 the coherence. Figures 5 and 6 display the line pixels extracted with the MRF method. The result shown in Figure 5 is based on intensity data only. It can be seen that it does not contain the pipelines in the lower half of the image where they cross a river. This is different when the extraction is based on a combination of intensity and coherence data as displayed in Figure 6.

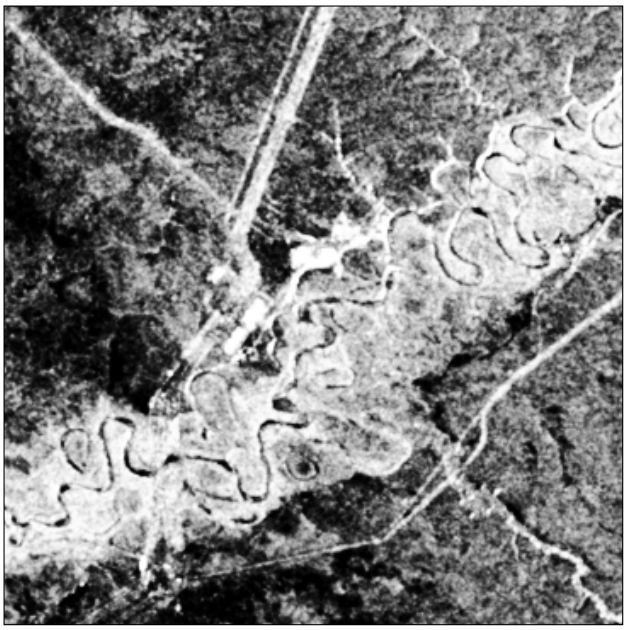

Figure 3: Multitemporal histogram-equalized magnitude of an ERS-SAR scene.

Figure 4: Multitemporal histogram-equalized coherence of an ERS-SAR tandem interferogram.

The posterior odds of the most probable line states versus the no-line states are shown in Figure 7. They combine the basic line information of intensity and coherence data, and are, therefore, input of the interactive ziplock snake-based pipeline extraction. Figures 8 and 9 show five extracted pipelines and roads superimposed to the magnitude and the coherence image. A careful visual inspection reveals that a correct extraction of the pipelines would not have been possible with one of the data sources alone. The magnitude does not contain any line information in the fluvial plain of the river, and the coherence does not show sufficient line information in the upper part of the image.

The ziplock method was of major importance for the suc-

Figure 5: Line pixels (black) and no-line pixels (white) extracted from intensity.

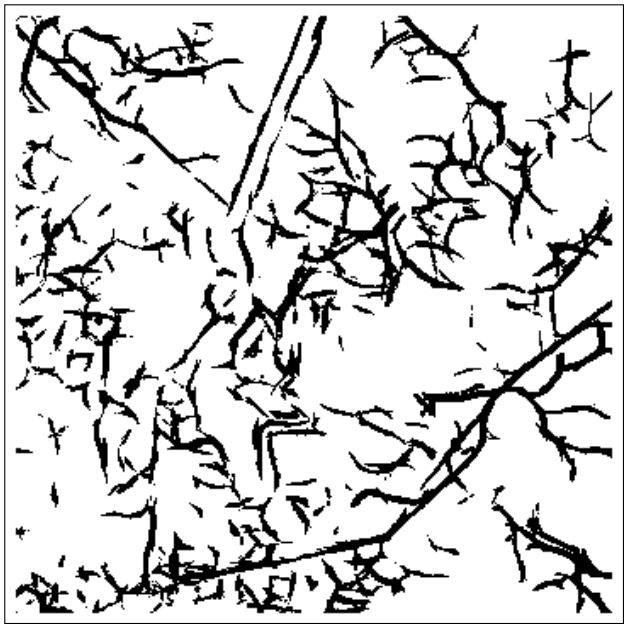

Figure 6: Line pixels (black) and no-line pixels (white) extracted from intensity and coherence.

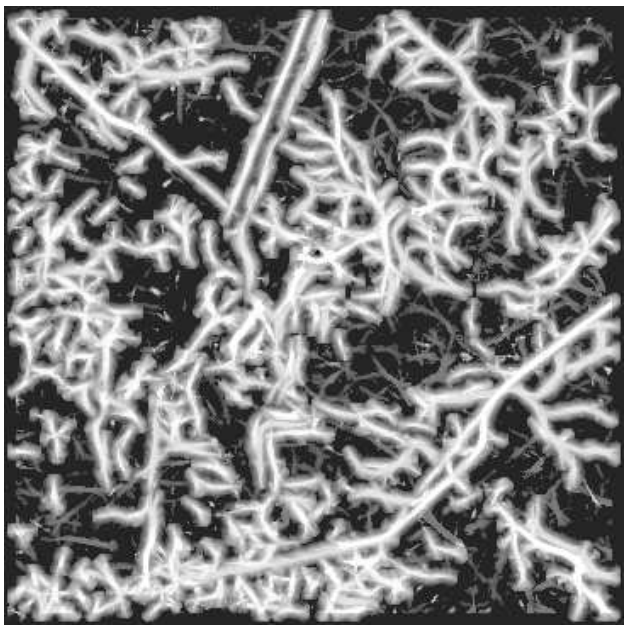

Figure 7: Posterior odds.

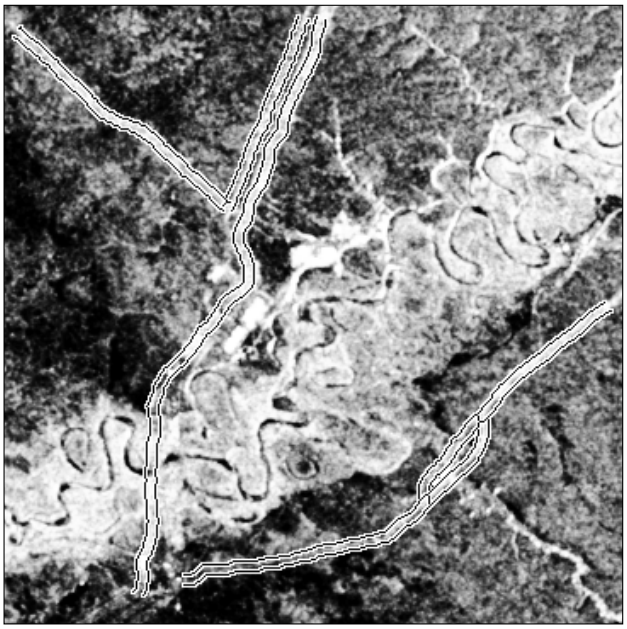

Figure 8: Pipelines and roads extracted with ziplock snakes from posterior odds superimposed to SAR magnitude.

cess of the ribbon snake-based extraction: Only by optimizing from the given ends inwards it was possible to track the pipeline avoiding to get stuck to other lines with high posterior odds.

5 CONCLUSIONS

The fusion of SAR intensity and interferometric SAR coherence data for line extraction using a Bayesian approach has been introduced. The new method applies an MRF model to suppress speckle-related line gaps. Results are line pixels with line directions and posterior odds showing the strength of the line state in comparison with the no-line state.

The posterior odds contain line information from both data sources. They can be used for further object extraction. Here, they have been input to a ziplock snake-based extraction of pipelines. Though, it would be desirable to conduct the extraction automatically, interactive processing was necessary to achieve reliable results. The reasons for difficulties of automatic processing are twofold. (1) Despite of the speckle suppressing effect of the MRF model, the posterior odds have a high noise level. They contain many structures which are caused by other objects than pipelines, e.g. by terrain features, which confuse automatic extraction. (2) The object model of the ziplock-snake

Figure 9: Pipelines and roads extracted with ziplock snakes from posterior odds superimposed to interferometric SAR coherence.

method has been developed for road extraction from optical images. It would possibly be more successful for automatic extraction, if it had been better adjusted to the appearance of the objects in its input derived from SAR data.

ACKNOWLEDGMENTS

The authors thank Kayser-Threde GmbH, München, for providing the SAR data.

REFERENCES

Caves, R., 1993. Automatic Matching of Features in Synthetic Aperture Radar Data to Digital Map Data. Dissertation, University of Sheffield, Dept. of Applied and Computational Mathematics.

Chou, P. B., Cooper, P. R., Swain, M. J., Brown, C. M. and Wixson, L. E., 1993. Probabilistic Network Inference for Cooperative High and Low Level Vision. In: R. Chellappa and A. Jain (eds), Markov Random Fields. Theory and Applications, Academic Press, Boston, pp. 211–243.

Fua, P. and Leclerc, Y., 1990. Model Driven Edge Detection. Machine Vision and Applications 3, pp. 45–56.

Geman, D. and Geman, S., 1984. Stochastic Relaxation, Gibbs Distribution, and the Bayesian Restoration of Images. IEEE Transactions on Pattern Analysis and Machine Intelligence PAMI-6(6), pp. 721–741.

Goodman, J. W., 1975. Statistical Properties of Laser Speckle Patterns. In: J. C. Dainty (ed.), Laser Speckle and Related Phenomena, Topics in Applied Physics, Vol. 9, Springer, Berlin, pp. 9–74.

Hellwich, O., 1997. Linienextraktion aus SAR-Daten mit einem Markoff-Zufallsfeld-Modell. Reihe C, Vol. 487, Deutsche Geodätische Kommission, München.

Hellwich, O., 1998. Model Parameter Estimation Using Simulated Annealing. ISPRS Commission III Symposium, Columbus, Ohio, in print.

Hellwich, O. and Streck, C., 1996. Linear Structures in SAR Coherence Data. In: International Geoscience and Remote Sensing Symposium 96, Lincoln, Vol. I, IEEE, pp. 330–332.

Hendry, A., Quegan, S. and Wood, J., 1988. The Visibility of Linear Features in SAR Images. In: International Geoscience and Remote Sensing Symposium 88, Edinburgh, IEEE, pp. 1517–1520.

Kass, M., Witkin, A. and Terzopoulos, D., 1987. Snakes: Active Contour Models. International Journal of Computer Vision 1(4), pp. 321–331.

Koch, K.-R., 1990. Bayesian Inference with Geodetic Applications. Lecture Notes in Earth Sciences, No. 31, Springer-Verlag, Berlin.

Laptev, I., 1997. Road Extraction Based on Snakes and Sophisticated Line Extraction. Master's thesis, Computational Vision and Active Perception Lab (CVAP), Royal Institute of Technology, Stockholm, Schweden.

Leberl, F. W., 1990. Radargrammetric Image Processing. Artech House, Norwood, MA.

Lopes, A., Nezry, E., Touzi, R. and Laur, H., 1993. Structure Detection and Statistical Adaptive Speckle Filtering in SAR Images. International Journal of Remote Sensing 14(9), pp. 1735–1758.

Neuenschwander, W., Fua, P., Székely, G. and Kübler, O., 1995. From Ziplock Snakes to Velcro^{TM} Surfaces. In: Automatic Extraction of Man-Made Objects from Aerial and Space Images, Birkhäuser Verlag, Basel, Schweiz, pp. 105–114.

Tough, R. J. A., Blacknell, D. and Quegan, S., 1994. Polarimetric Radar: Mathematical Models and their Consequences. In: 3rd draft version, 17.03.94, submitted to the Proceedings of the Royal Society.

Williams, L. and Jacobs, D., 1995. Stochastic Completion Fields: A Neural Model of Illusory Contour Shape and Saliency. In: Fifth International Conference on Computer Vision, pp. 408–415.

Winkler, G., 1995. Image Analysis, Random Fields and Dynamic Monte Carlo Methods. Applications of Mathematics, Vol. 27, Springer-Verlag, Berlin.